JOURNAL OF COMPUTATIONAL PHYSICS 9, 398–411 (1972)

Numerical Aspects of Momentum-Space Scattering Equations for Peaked Potentials*

MICHAEL L. ADELBERG AND ALVIN M. SAPERSTEIN

Department of Physics, Wayne State University, Detroit, Michigan 48202

Received June 8, 1971

Several programming techniques are suggested for solving partial wave scattering equations in momentum space when the potential matrix, as a function of momentum variables, is strongly peaked about the scattering singularity. In particular, an algorithm is described that makes use of the second Born approximation to estimate error in performing principal value quadratures. For a given required accuracy, one obtains a region of integration about the singularity and a Gauss–Legendre quadrature on this region whose truncation error equals the error due to discarding the region away from the singularity and whose order is much lower than that required by full region quadrature to get the same accuracy. Considerable saving in computer time is achieved.

I. INTRODUCTION

There has been recent and extensive interest in solving scattering equations in momentum space for several energy ranges, including the low-energy Fadeev equations [1], intermediate-energy optical models [2], and high-energy pseudopotentials [3]. The essential idea of all these approaches is to reduce the Lippmann–Schwinger equations to a Fredholm-type integral equation with a compact kernal [4]. Under slightly more restrictive conditions, it has been shown that the kernal can be represented by a matrix of finite rank, so that the problem becomes one of solving a system of simultaneous linear equations.

In this paper, elementary but useful numerical aspects are discussed for scattering equations in momentum space when the potential is rotationally invariant, reciprocal, smooth, and very peaked, so that in terms of the momentum-space representative,

$$\langle \mathbf{p}' \mid V \mid \mathbf{p} \rangle = V(p', p, q), \qquad \mathbf{q} = \mathbf{p}' - \mathbf{p}, \tag{1}$$

$$\langle \mathbf{p}' \mid V \mid \mathbf{p} \rangle = \langle -\mathbf{p} \mid V \mid -\mathbf{p}' \rangle, \tag{2}$$

$$V(p', p, q) \not\approx 0 \qquad \text{only when} \quad p' \approx p,\ p \approx k \text{ or } p < k, \text{ and } q/k \approx 0, \tag{3}$$

* Work supported in part by the National Science Foundation under grant number GP-7853.

where k is the center-of-mass momentum at the incident energy E. These conditions hold at intermediate and higher energies for nuclear optical models and elementary particle potentials. The primary purpose of this paper is to show how, for such potentials, observables can be very rapidly calculated to an accuracy easily within that warranted by experimental data.

An algorithm is presented which is most useful for potentials,

$$V(p', p, q; E) = v(p', p, q; E) F(q), \tag{4}$$

whose major characteristic is that the shape [i.e., the strong peaking described by (3)] is primarily determined by the form factor F, which does not change over a series of runs. One can then examine the effect on the observables caused by varying parameters from which v is constructed. For example, in nucleon–nucleus impulse potentials, the form factor is well determined experimentally by electron–nucleus scattering; the quantities to be varied—which determine v—are the nucleon–nucleon phase parameters and the off-shell extensions to the nucleon T-matrix. Here, the shape of the potentials is dominated by the form factor and it thus becomes worthwile to exert some effort to obtain an accurate yet efficient numerical procedure, which can then be used for many similar potentials, differing slightly in shape due to variations in v.

In the exposition, the scattering equations are written only for the spin-zero case; moreover, a detailed numerical analysis is made only for the example of a real Gaussian potential. However, we stress that it is not necessary to assume that the potential is local, real, or spin independent. In particular, we note at the conclusion the results for a realistic nucleon–nucleus optical potential that is nonlocal, complex, and spin dependent. In fact, use of momentum-space equations is most advantageous for nonlocal potentials because no localization approximation (which is invoked ad hoc. so as to avoid solving an integrodifferential equation) need be performed. In momentum space, locality has no special role, and the peakedness of the potentials at energies above 100 MeV is overwhelmingly their most significant numerical feature. In addition, the potentials have often been evaluated in momentum space and then Fourier transformed into coordinate space; this is both wasteful and unnecessary.

II. Momentum-Space Scattering Equations

When there is no spin, an angular-momentum decomposition of the single-channel, nonrelativistic, Lippmann–Schwinger equation gives [5]

$$T_l(z, z') = V_l(z, z') + \frac{2}{\pi} \int_0^\infty \frac{dz'' z''^2}{1 + i\epsilon - z''^2} V_l(z, z'') T_l(z'', z'), \tag{5}$$

where T_l and V_l are angular-momentum partial wave projections of the momentum-space matrix elements of the barycentric operators T and V. All quantities are unitless so that the elastic cross section is given by

$$\sigma(\theta) = \left| \sum_l C_l T_l(1, 1)/k \; P_l(\cos\theta) \right|^2, \qquad C_l = 2l + 1, \tag{6}$$

where P_l are Legendre polynomials and z, z', z'' are ratios of the momentum variables to their on-shell value k. (All omitted arguments have the value 1.) The only physically relevant matrix element is T_l, but in order to obtain it, one must solve the Fredholm equation [5], for the half-shell vector:

$$T_l(z) = V_l(z)(1 - iT_l) + \frac{2}{\pi} \mathbf{P} \int_0^\infty \frac{dz' z'^2}{1 - z'^2} V_l(z, z') \, T_l(z'), \tag{7}$$

where **P** stands for Cauchy principal value. In practice, this is accomplished by selecting a finite set of points to represent the momentum variable so that (7) becomes a system of simultaneous equations. Henceforth, we shall omit writing the angular-momentum index, l.

Actually, (7) is inconvenient both for analysis and computation because it is complex even for real potentials and it includes the singular point, $z = 1$. By simple transformations, it is possible to write equivalent equations for the reaction matrix and the half-off-shell factor obtained by Fredholm reduction [6]

$$R(z) = V(z) + \frac{2}{\pi} \mathbf{P} \int_0^\infty \frac{dz' z'^2}{1 - z'^2} V(z, z') \, R(z'), \tag{8}$$

$$H(z) = V(z)/V + \frac{2}{\pi} \int_0^\infty \frac{dz' z'^2}{1 - z'^2} [V(z, z') - V(z) \, V(z')/V] \, H(z'). \tag{9}$$

These functions are related to the scattering matrix by

$$H(z) = T(z)/T = R(z)/R \tag{10}$$

and

$$T = R/(1 + iR). \tag{11}$$

Equation (9) is not singular, and the singularity of (8) presents no difficulty, in our example, for energy greater than 50 MeV, while in both equations the value $z = 1$ is excluded. The phase shifts are obtained from (8) and (11) by using

$$R = V + \Pi \tag{12}$$

with

$$\Pi = \frac{2}{\pi} \mathbf{P} \int_0^\infty \frac{dz\, z^2}{1 - z^2} V(z)\, R(z). \tag{13}$$

The principal value quadrature in (13) yields the numbers Π_l which, along with the V_l, provide the total physical content of the elastic scattering. Thus, *assuming* that the numerical angular-momentum projection yielding $V_l(z, z')$ is performed with reasonable accuracy and efficiency, the speed and error obtained in calculating the observables is determined by the technique used to solve (8) and then perform (13).

III. Principal Value Quadrature

It is possible to subtract out the singularity that occurs in (13) by breaking the range of the integration variable into (0, 1) and (1, ∞) and then mapping the latter into the former by the transformation $1/z$, so that one obtains

$$\Pi = \frac{2}{\pi} \int_0^1 \frac{dz}{1 - z^2} [z^2 V(z)\, R(z) - V(1/z)\, R(1/z)/z^2]. \tag{14}$$

This procedure has the advantages of being easy to apply to integrands whose functional form is unknown when quadrature points are selected and of simultaneously handling the singular nature of (8). Therefore, a set, z_i, including points in (0, 1) and their reciprocals in (1, ∞) are selected to represent the momentum variable, along with $z = 1$ which is excluded from the set. For any such choice, the quadrature (14) is approximated by the sum,

$$\Pi = \sum_{i=1}^{n} \left(\frac{w_i}{1 - z_i^2}\right) \left[z_i^2 V(z_i)\, R(z_i) - \frac{1}{z_i^2} V\left(\frac{1}{z_i}\right) R\left(\frac{1}{z_i}\right)\right], \tag{15}$$

where the weight w_i depends on the quadrature rule employed. The accuracy, even for a given n, with which (15) evaluates the principal value, depends very sensitively on the selection of points.

IV. Symmetric-Matrix Equation

One can make use of the symmetry imposed upon $V(z, z')$ by reciprocity to obtain a system of simultaneous linear equations whose matrix of coefficients is symmetric. First, define a diagonal matrix D whose i-th diagonal element is $+1$

when $z_i > 1$ and -1 when $z_i < 1$. Now define the elements of the vectors and matrix to be

$$W_i = D_{ii}\left[\frac{2}{\pi}(w_i z_i^2)/(1 - \hat{z}_i^2)\right]^{1/2}, \qquad \hat{z}_i = \min(z_i, 1/z_i), \tag{16}$$

$$V_i = W_i V(z_i), \tag{17}$$

$$R_i = |W_i| R(z_i), \tag{18}$$

$$V_{ij} = W_i W_j V(z_i, z_j). \tag{19}$$

With the above definitions, (8) and (13) become

$$\sum_{j=1}^{N} (D_{ij} + V_{ij}) R_j = V_i \tag{20}$$

and

$$\Pi = -\sum_{i=1}^{N} V_i R_i, \tag{21}$$

respectively, where $N = 2n$. The reason for maintaining the symmetry in (20) is that, for real V_{ij}, approximately $N^3/3$ multiplicative operations are needed to obtain a solution in general, but only $N^3/6$ when the matrix of coefficients is symmetric [7]. When the potential is complex the fastest available algorithms require about 2^3 times as many multiplicative operations as in the real case. It is therefore an economic necessity to keep N as small as possible in order to keep computing costs within reason.

Furthermore, for large N, floating-point rounding errors can lead to large errors in the solution. Typical estimates [8] of this error indicate that it is proportional to the rounding error per operation (about 10^{-7} single precision for IBM System 360), to some power between 2 and 3 of the order of the system of equation, and to the condition of the matrix of coefficients. This last number is defined as the square root of the ratio of the largest to smallest eigenvalue of the product of the matrix and its Hermitian conjugate. When using an algorithm to solve (8) symmetrically, it is particularly important that the matrix be well conditioned (here the condition times N^2 should be much less than 10^7) because symmetry must be maintained at each step so that pivoting is allowed only along the main diagonal [9]. In our example, at the higher E *or* higher l, the matrices, $D + V$, are diagonally dominant and have conditions near unity. Even at the lowest E considered for $l = 0$, the solution of (20) is accurate (as verified by back substitution) to at least four decimal places.

V. Quadrature Algorithm

It is difficult to numerically integrate (14) because the peaking of the functions in the integrand is different on either side of $z = 1$. The standard rules of Gaussian quadrature do not work well over the whole region (0, 1); in fact, 4- and 8-point midpoint rules out-perform Gauss–Legendre [10] rules of the same order. In this section, we present a heuristic procedure for obtaining a quadrature rule that is both efficient and accurate.

First, to measure accuracy, we give the following definition of error:

$$X = \| \mathbf{\Pi} - \mathbf{\Pi}_A \| / \| \mathbf{\Pi} \|, \tag{22}$$

where $\mathbf{\Pi}_A$ is the value of (15) produced by our algorithm and $\mathbf{\Pi}$ is the "exact" value of (14) (as calculated by a higher-order quadrature). All vectors in (22) and subsequently are indexed by angular momentum and the vector norm is defined as

$$\| \mathbf{\Pi} \| = \sum_l C_l \, | \Pi_l | . \tag{23}$$

The purpose of our procedure is to provide an estimate for X so as to allow the most efficient program for a given upper bound on X. However, it is stressed that X can only be found by solving (20) for $\mathbf{\Pi}$ and $\mathbf{\Pi}_A$.

Next, to estimate X, we use the first- and second-order Born approximations to the phase shift which, respectively, are given by

$$R \approx V, \tag{24}$$

$$\Pi \approx Q, \tag{25}$$

where

$$Q = \frac{2}{\pi} \int_0^1 \frac{dz}{1 - z^2} [z^2 V^2(z) - V^2(1/z)/z^2]. \tag{26}$$

The first approximation (24) is good when V is small, i.e., high energy of large l, while the second (25) gives only an order of magnitude for low energy or small l. The usefulness of Eqs. (24)–(26) is that they give a fair estimate of the shape of the exact integrand (14), and—in estimating the accuracy of integration procedures—it is shape and not magnitude of the integrand that counts. The algorithm makes use of the peakedness of the integrand of (26) by simply discarding the region of integration that does not contribute significantly to the quadrature. The discard error, caused in the evaluation of Q, is given by

$$X_D(z_0) = \| \mathbf{Q}_M(0) - \mathbf{Q}_M(z_0) \| / \| \mathbf{Q}_M(0) \|, \tag{27}$$

where $\mathbf{Q}_M(z_0)$ is found by subtracting pairs of values [as in (15)] from $\mathbf{Q}_M(0)$, which is evaluated with a 25-point midpoint rule; thus, $\mathbf{Q}_M(z_0)$ are evaluations of (26) on the intervals $(z_0, 1)$. Also, on these intervals, evaluations are made using several orders (labelled by n) of Gauss–Legendre. The truncation error is defined to be

$$X_T{}^n(z_0) = \| \mathbf{Q}(z_0) - \mathbf{Q}_n(z_0)\| / \| \mathbf{Q}(z_0)\|. \tag{28}$$

This error is an estimate of how well the Gauss–Legendre rule can be expected to perform the quadratic (26) on the interval $(z_0, 1)$. Here, $\mathbf{Q}(z_0)$ is presumed to be "exact" and is obtained using the largest order considered; we used up to 32 points, but this is excessive when only single precision is used; 16 points are entirely adequate.

The basic assumption made—to be justified in the next section by examination of a numerical example—is that the sum of $X_T{}^n(z_0)$ and $X_D(z_0)$ is a good estimate of X when n and z_0 are chosen so that $X_T{}^n(z_0) \leqslant X_D(z_0)$. In other words, a good representation of $\mathbf{Q}$ implies $\mathbf{\Pi}$ is well represented. Furthermore, there is no point to having a truncation error less than the discard error; the latter can be very small, even for large values of z_0, because of the rapid fall-off of the potential. Large z_0 means a small region $(z_0, 1)$ so that relatively few Gaussian points are needed for acceptable truncation errors; in fact, considerably fewer are needed than would be needed to give the same truncation error over the entire interval (0, 1). The points of intersection of the curves for the $X_T{}^n(z_0)$ with $X_D(z_0)$ are labeled Z_n; thus, the algorithm finds, in addition to the error estimate of $2X_D(Z_n)$, an interval $(Z_n, 1)$ on which n-th order Gauss–Legendre quadrature is to be performed.

VI. Numerical Example

In this section, the usefulness of the algorithm just described is demonstrated for a Gaussian potential used to represent intermediate energy $n - C$ elastic scattering [11]. In momentum space this potential is

$$V(q) = V_0' e^{-(\frac{1}{2}bq)^2}, \tag{29}$$

where $V_0' = 2\mu k\pi^{1/2}1/4b^3V_0$, $b = 2.85$ F, $V_0 = -33.1$ MeV, and μ is the reduced nucleon mass. Expressing the square of momentum transfer in the exponential in terms of k, z, and z', the reduced matrix elements are given by

$$V_l(z, z') = V_0' e^{-a(z-z')^2} \int_0^\pi d\theta \sin\theta \, P_l(\cos\theta) \, e^{-2azz'(1-\cos\theta)}, \qquad a = (1/2kb)^2, \tag{30}$$

where the normalization is consistent with (8) and (20). The exponential factor in front of the integrand is primarily responsible for the strong peaking, while the integral goes as $(zz')^l$ as z or z' approaches zero.

In Fig. 1, at 25, 50, 100, 200, and 400 MeV, X_D is drawn with solid lines, while $X_T{}^n$ are drawn with dashed, dash-dot, and dotted lines for $n = 4$, 8, and 16, respectively. The intersections, Z_n, at each energy, of the curves are indicated by solid circles. As a first check on the algorithm, $\mathbf{\Pi}$ and $\mathbf{\Pi}_A$ were calculated with (20)

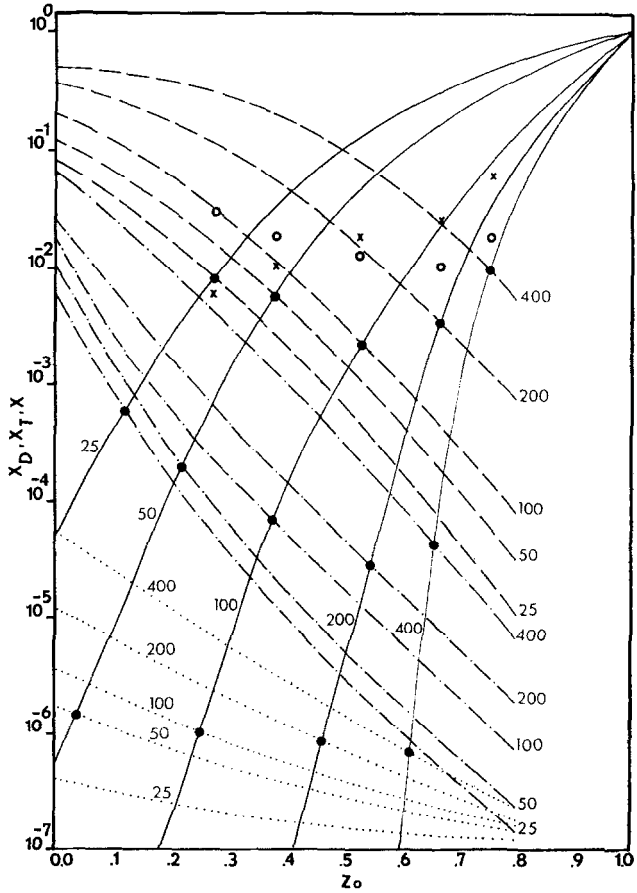

FIG. 1. Discard and truncation errors as a function of integration interval and incident energy: $X_D(z_0)$ are drawn with solid lines, while $X_T{}^n(z_0)$ are drawn with dashed, dash-dot, and dotted lines, for $n = 4$, 8, 16, respectively. The intersections, Z_n, are indicated by solid circles. Open circles are the values of X at the energies corresponding to Z_n, while the small x's are the values of $X_T{}^8(0)$.

and (21) using the Gauss–Legendre rules on $(Z_8, 1)$ and $(Z_4, 1)$, respectively. At each Z_4 position, the value of X resulting from (25) is indicated by an open circle and $X_T^8(0)$ is indicated by a small x. The figure shows that the discard and truncation errors, which are defined in the second Born approximation, give a good estimate of X, which is obtained only after the equations (20) are solved. Furthermore, above 100 MeV, the open circles lie below the corresponding x, so that *better accuracy as well as superior efficiency can be expected of these four-point rules than of the full range eight-point rules.* Similar comparison of the 8- and

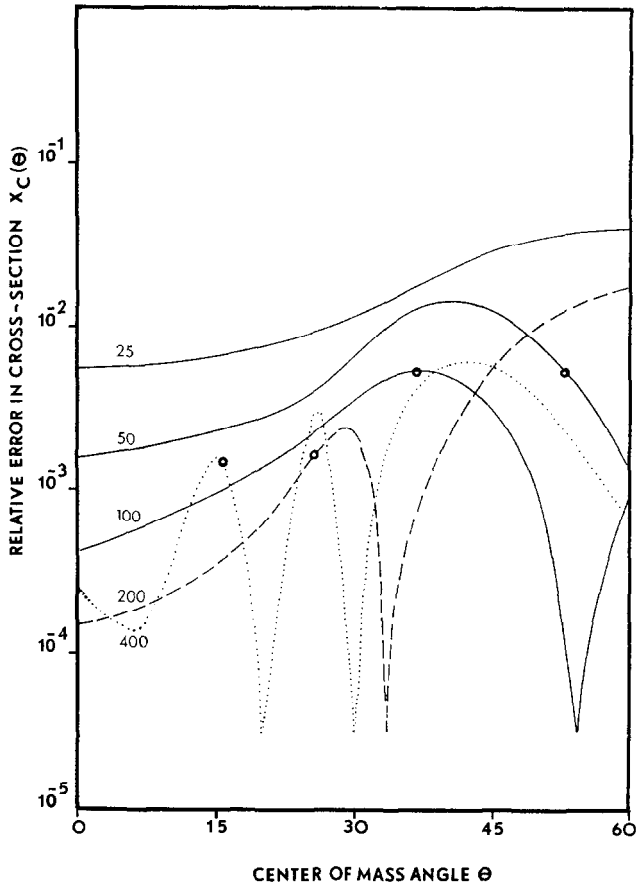

FIG. 2. Error in cross section as a function of center-of-mass angle and incident energy: $X_C(\theta)$ are drawn with solid lines for energies of 25, 50 and 100 MeV, and with dashed and dotted lines at 200 and 400 MeV, respectively. Open circles indicate the position of the diffraction minimum.

16-point rules on the graph indicates that the truncation error of the full-range 16-point rule is roughly the same as the total error of our 8-point rule. In fact, above 400 MeV the full-range procedures soon give truncation errors in excess of 20 % while the amputated-range algorithm remains accurate to within a few percent up to 1600 MeV. The $n = 4$ and $n = 8$ curves were smoothed somewhat to improve legibility; straight lines were drawn through the $z_0 = 0$ and $z_0 = 0.1$ points to indicate the trends of the $n = 16$ curves, which tended to oscillate wildly. This oscillation occurs even with double precision calculations because, even on the same interval, different-order Gaussian quadratures use completely different sets z_i. The numerical-decomposition procedure used to obtain the vectors V_i was accurate at best to five decimal places, so that below the 10^{-5} line the truncation error curves are not reliable.

In Fig. 2, the relative error in the cross section,

$$X_C(\theta) = |\sigma(\theta) - \sigma_A(\theta)|/\sigma(\theta), \tag{31}$$

is drawn as a function of angle for the energies in Fig. 1. Here, $\sigma(\theta)$ and $\sigma_A(\theta)$ are calculated from the $\mathbf{\Pi}$ and $\mathbf{\Pi}_A$ just obtained. Even at very large angles (well beyond the first diffraction minimums which are indicated by open circles), $X_C(\theta)$ lie well below the corresponding values of X or even of $X_T{}^4(Z_4) = X_D(z_4)$. Hence, in this example, the discard error itself provides a useful estimate of the error involved in computing observables like differential cross section. Similar results have been obtained for real and complex harmonic potentials that have been used to describe intermediate energy $n - C$ scattering. The eight-point solution for 100 MeV Gaussian and harmonic potentials has been compared with the exact partial wave coordinate space calculation used in [11]; on a log plot, no discrepancy can be seen up to and just beyond the first diffraction minimum.

VII. Further Suggestions and Remarks

Other Programming Steps

This paper has concentrated on keeping the numbers of points, $N + 1 = 2n + 1$, used to represent the momentum variable z, to a practical minimum and on the solution step in the program, whose computation time is proportional to N^3. Essentially all the remaining computer time is consumed in setting up the potential and taking its angular decomposition. Let L be the number of partial waves that contribute significantly to the scattering amplitude and let M be the number of

angles at which the input potential matrix is to be computed. Then, for real potentials, the following are estimates of the computation time for each step:

SET-UP:	SN^2Mn_{op} ;	(32)
DE-COMP:	SN^2ML;	(33)
SOLVE:	$SN^3/6L$.	(34)

Here, S is 1/2 when the potential is symmetric, 1 otherwise, and n_{op} is the number of multiplicative operations needed to set up each potential matrix element. If full use of symmetry is made, 50 % of computation time is saved: use of our algorithm to half N saves an additional 75 % of what remains.

Reduction of M in the Decomposition

This saving of 85 % of computational time for a given fixed accuracy should be adequate for most budgets. However, the potentials that are peaked in momentum variables are also strongly peaked in angle. In our example, the back hemisphere does not contribute to the first four places of V_l for energy greater than 100 MeV. Furthermore, as is the case for the principal value quadrature, a straightforward numerical decomposition integration becomes decreasingly accurate as energy increases since the distribution becomes more peaked. It seems likely that a similar algorithm can be found to reduce M with either no change or even an increase in accuracy; however, this is complicated by the fact that the vector V_i and the matrix V_{ij} as well as the single element V_l must be calculated by the given angular decomposition procedure.

A Realistic Example: Complex, Nonlocal, and Spin Dependent

The above numerical analysis came about as a result of an attempt to extend the work of Chalmers and Saperstein [12] in order to investigate the effect on intermediate energy nucleon-nucleus cross section and polarization of taking the nucleon T-matrix off its energy shell. The potentials used by these authors were evaluated and their scattering equations were solved in momentum space. In addition to being complex and spin dependent, these potentials are nonlocal, so that the use of momentum-space scattering equations is particularly advantageous. In [12] scattering equations based on (7) using tenth-order Gauss–Legendre quadrature were solved using 21 points to represent the momentum variable in their matrices ($z = 1$ was included). The resulting real matrices were 42 by 42 since the complex matrix equation that comes from (7) has the form

$$(A + iB)(x + iy) = a + ib, \tag{35}$$

which leads to the real matrix equation,

$$\begin{pmatrix} A & -B \\ B & A \end{pmatrix}\begin{pmatrix} x \\ y \end{pmatrix} = \begin{pmatrix} a \\ b \end{pmatrix}. \tag{36}$$

On the Model 67 of IBM System 360, this original program, whose input was on and off shell nucleon–nucleon phase parameters, form-factor constants, etc., and whose final output was cross section and polarization, required over five min CPU time.

With the algorithm described here, using the reaction-matrix formulism to yield symmetric complex matrices, $A' + iB'$, and the corresponding vectors as indicated in Section IV and handling these complex matrices by the following more efficient alternative to (36), the run time was reduced to less than 11 sec CPU time. Probably the best way to solve the symmetric equation equivalent to (35) is to first find the matrix solution to $A'C = B'$, whose transpose is equal to $B'A'^{-1}$, and use this result in

$$[A' + (B'A'^{-1})\,B'](x' + iy') = [1 - i(B'A'^{-1})](a' + ib'), \tag{37}$$

fully exploiting the symmetry of (37). This procedure takes the same number of multiplicative operations as the symmetric version of (36),

$$\begin{pmatrix} A' & B' \\ B' & -A' \end{pmatrix}\begin{pmatrix} x' \\ y' \end{pmatrix} = \begin{pmatrix} a' \\ b' \end{pmatrix}, \tag{38}$$

but is more accurate and faster because less pivoting occurs in performing the triangular decomposition of two N-th order matrices than of one $2N$-th order equation.

For $n - C$ scattering at 142 MeV, the new procedure using $n = 4$ reproduces to within 2 % those T_l that resulted from the old procedure with $n = 10$, and the cross section and polarization are nearly indistinguishable at less than 45° center-of-mass scattering angle. At 310 MeV ($p - C$), there is a significant difference in the value of the polarization at the diffraction minimum (23°); this value is proportional to the difference of the nearly equal spin-flipped and not-flipped cross sections; however, this value is very poorly determined experimentally, so that the numerical difference just noted was less than half the experimental uncertainty. Our work indicates that the faster procedure is also the more accurate, because the truncation error of the full-range 10-point rule is larger than that of the optimum 4-point rule.

Energy Below 50 MEV

We have concentrated on intermediate energies and found the techniques suggested in this paper to be adequate for strongly peaked potentials. At energies below

50 MeV, even our Gaussian example becomes reasonably flat so that breaking the interval $(0, \infty)$ into $(0, 1)$ and $(1, \infty)$ may not be preferable to using an even-order Gaussian quadrature on an interval $(0, 2)$ symmetric about the pole $z = 1$ and evaluating the integral on $(2, \infty)$ with some other rule [13]. Furthermore, the first Born approximation is very poor (i.e., Π_l is of the same order of magnitude as V_l) for the few partial waves that contribute to the scattering amplitude, so that the principal values must be calculated to at least three-place accuracy, if the resulting R_l are to be good to two places. Finally, at these low energies, the matrices $D + V$, which come from (8) are not sufficiently well behaved to give better than three-place accuracy; however, the matrix equations arising from (9) are probably far more accurate; work at 142 MeV for complex potentials has shown the solutions to the Fredholm reduced equations are over one place more accurate than those of the R-matrix equation (20), since the condition of the resulting Fredholm matrix is smaller than that of the comparable R-matrix.

Energy Above 400 MEV

At higher energies very many [15] partial waves contribute significantly to the scattering amplitude; the $V_l(z)$ become so very strongly peaked—even on the intervals $(Z_n, 1)$—that Gauss–Legendre quadrature becomes very inefficient. Preliminary investigation indicates that other types of Gaussian quadrature [14] then become more efficient. The use of the second Born approximation to the phase shift (25) has been investigated [15] and found useful for the larger l included in the decomposition. Our own investigation shows that at each energy in our example both the Q_l and Π_l change sign at the same l. Before this change occurs the Q_l overestimates the Π_l greatly; afterwards, the approximation (25) soon is quite good. At high energies many partial waves are still significant after the change in sign occurs, so that this approximation is useful. Finally, the numerical decomposition of the potential into partial waves is difficult and the resulting decomposed elements should be checked for accuracy.

References

1. I. H. Sloan, *Phys. Rev.* **165** (1968), 1587.
2. J. S. Chalmers and A. M. Saperstein, *Phys. Rev.* **168** (1968), 1145.
3. C. Itzykson, V. G. Kadyshevsky, and I. T. Todorov, *Phys. Rev.* **1D** (1970), 2823.
4. K. M. Watson and J. Nuthall, "Topics in Several Particle Dynamics," Chapter 1, Holden-Day, New York, 1967.
5. M. L. Goldberger and K. M. Watson, "Collision Theory," Chapter 6, John Wiley & Sons, New York, 1964.
6. H. P. Noyes, *Phys. Rev. Lett.* **15** (1965), 538.
7. G. E. Forsythe and C. B. Moler, "Computer Solution of Linear Algebraic Systems," Section 9, Prentice-Hall, Englewood Cliffs, NJ, 1967.

8. G. E. FORSYTHE AND C. B. MOLER, "Computer Solution of Linear Algebraic Systems," Section 21, Prentice-Hall, Englewood Cliffs, NJ, 1967.
9. IBM Publication H20-0205-1, SYSTEM/360 Scientific Subroutine Package, p. 182, IBM Technical Publications Department, White Plains, NY, 1967.
10. P. J. DAVIS AND P. RABINOWITZ, "Numerical Integration," p. 33, Blaisdell, Toronto, 1967.
11. Y. NISHIDA, M. SHIMAUCHI, AND H. TANAKA, *Nucl. Phys.* **50** (1964), 403.
12. J. S. CHALMERS AND A. M. SAPERSTEIN, *Phys. Rev.* **156** (1967), 1099.
13. I. H. SLOAN, *J. Comput. Phys.* **3** (1968), 332.
14. M. ABRAMOWITZ AND I. A. STEGUN (Eds.), "Handbook of Mathematical Functions," pp. 921–924, Natl. Bureau of Standards Appl. M. Series 55, 1964.
15. T. A. OSBORN, private communication.